



This is a repository copy of *Design and optimization of cold-formed steel sections in bolted moment connections considering bimoment*.

White Rose Research Online URL for this paper:  
<http://eprints.whiterose.ac.uk/172624/>

Version: Accepted Version

---

**Article:**

Phan, D.T., Mojtabaei, S.M., Hajirasouliha, I. [orcid.org/0000-0003-2597-8200](https://orcid.org/0000-0003-2597-8200) et al. (2 more authors) (2020) Design and optimization of cold-formed steel sections in bolted moment connections considering bimoment. *Journal of Structural Engineering*, 146 (8). 04020153. ISSN 0733-9445

[https://doi.org/10.1061/\(asce\)st.1943-541x.0002715](https://doi.org/10.1061/(asce)st.1943-541x.0002715)

---

This material may be downloaded for personal use only. Any other use requires prior permission of the American Society of Civil Engineers. This material may be found at [https://doi.org/10.1061/\(ASCE\)ST.1943-541X.0002715](https://doi.org/10.1061/(ASCE)ST.1943-541X.0002715)

**Reuse**

Items deposited in White Rose Research Online are protected by copyright, with all rights reserved unless indicated otherwise. They may be downloaded and/or printed for private study, or other acts as permitted by national copyright laws. The publisher or other rights holders may allow further reproduction and re-use of the full text version. This is indicated by the licence information on the White Rose Research Online record for the item.

**Takedown**

If you consider content in White Rose Research Online to be in breach of UK law, please notify us by emailing [eprints@whiterose.ac.uk](mailto:eprints@whiterose.ac.uk) including the URL of the record and the reason for the withdrawal request.



[eprints@whiterose.ac.uk](mailto:eprints@whiterose.ac.uk)  
<https://eprints.whiterose.ac.uk/>

# Design and Optimization of Cold-Formed Steel Sections in Bolted Moment Connections Considering Bimoment

Duoc T. Phan<sup>1</sup>, Seyed Mohammad Mojtabaei<sup>2</sup>, Iman Hajirasouliha<sup>3</sup>, T.L. Lau<sup>4</sup>, James B.P. Lim<sup>5</sup>

<sup>1</sup>Assistant Professor, Dept. of Civil Engineering, Faculty of Engineering and Science, Univ. of Nottingham Malaysia.

ORCID: <https://orcid.org/0000-0003-4410-9529>. Email: [duoc.phan@nottingham.edu.my](mailto:duoc.phan@nottingham.edu.my)

<sup>2</sup>Ph.D. Student, Dept. of Civil and Structural Engineering, Univ. of Sheffield, Sheffield, UK (corresponding author).

ORCID: <https://orcid.org/0000-0002-4876-4857>. Email: [smmojtabaei1@sheffield.ac.uk](mailto:smmojtabaei1@sheffield.ac.uk)

<sup>3</sup>Senior Lecturer, Dept. of Civil and Structural Engineering, Univ. of Sheffield, Sheffield, UK. ORCID:

<https://orcid.org/0000-0003-2597-8200>. Email: [i.hajirasouliha@sheffield.ac.uk](mailto:i.hajirasouliha@sheffield.ac.uk)

<sup>4</sup>Assistant Professor, Dept. of Civil Engineering, Faculty of Engineering and Science, Univ. of Nottingham Malaysia.

ORCID: <https://orcid.org/0000-0003-1782-4746>. Email: [teckleong.lau@nottingham.edu.my](mailto:teckleong.lau@nottingham.edu.my)

<sup>5</sup>Associate Professor, Dept. of Civil and Environmental Engineering, Univ. of Auckland, Auckland, New Zealand.

ORCID: <https://orcid.org/0000-0001-9720-8518>. Email: [james.lim@auckland.ac.nz](mailto:james.lim@auckland.ac.nz)

## Abstract

The load transfer mechanism in cold-formed steel (CFS) bolted moment connections is mainly through the bolt-group in the web of beam elements, which may lead to relatively large bimoment and warping deformation. While the bimoment effects can be considered in the Direct Strength Method (DSM), ignoring the bolt-group length in the conventional design process can lead to non-conservative solutions. This paper presents an alternative analytical design approach using Eurocode 3 (EC3) effective width method to determine the ultimate flexural strength of CFS bolted moment connections by considering bimoment effects. The results compare very well with previously published experimental test data as well as detailed finite element models developed in this study. It is shown that a short bolt-group length may lead to up to 25% reduction in the flexural strength of the CFS bolted connections. However, a longer bolt-group length generally results in a moment capacity almost equal to the flexural strength of the CFS channel section. Shape optimisation is then conducted using a Genetic Algorithm (GA) to improve the flexural capacity of the connections by taking into account the bimoment effects.

The main design variables are considered to be the relative CFS beam cross-sectional dimensions, while the plate slenderness and dimension limits suggested by EC3 as well as a number of manufacturing and practical end-use constraints are incorporated as design constraints. It is found that, compared with standard cross-sectional dimensions, the optimised sections can improve the flexural strength by as much as 36% for the bolt-group length equal to the depth of beam element.

## **Keywords**

Cold-formed steel (CFS); Bolted moment connection; Bimoment; Bolt-group length; Optimisation

## **1 Introduction**

The use of cold-formed steel (CFS) members as the main load-carrying structural members in portal frames and shear walls has significantly increased in the building industry. Compared to hot-rolled steel sections, CFS members have advantages such as a higher moment of inertia/weight ratio, ease of manufacturing, and flexibility in cross-sectional shape and dimensions. Manufacturing cross-sections with variety of shapes provides an opportunity to improve the behaviour of CFS structures (i.e. beam, column, beam-column, and frame) in terms of stiffness, strength, ductility and energy dissipation capacity (Mojtabaei et al., 2019, Ye et al., 2018a, Ye et al., 2018b, Wang et al., 2016, Phan et al., 2019).

Over the last decade, CFS moment-resisting frames have been increasingly used as the main structural system in the building industry. Previous studies indicate that the structural performance of a CFS moment-resisting frame depends mainly on the flexural behaviour of its connections (Mojtabaei et al., 2018, Lim and Nethercot, 2004a, Sabbagh et al., 2010, Dubina et al., 2009). The design of CFS beam and column members is generally carried out following the conventional approaches, i.e. Direct Strength Method (DSM) or Effective Width Method (EWM). However, experimental and analytical investigations on the moment-rotation behaviour and failure modes of different CFS bolted moment connections showed that flexural strength of the CFS sections may be also affected by eccentric bolts forces being

offset from shear centre, leading to warping torsion of the channel sections (Lim and Nethercot, 2003). This indicated that the flanges of the CFS beam sections should be accounted for the resulting warping torsion (or bimoment) at the connection zone. However, the bimoment effects are generally ignored in the conventional design of CFS moment-resisting frames.

For a channel section subjected to major axis moment, the bimoment leads to compression stresses at the top flange/web junction, which should be added to the compression stresses caused by major axis bending moment. Fig. 1 shows the stress profile for the combined stress distribution generated using CUFSM (Schafer, 2006). It can be seen that the bimoment generates tensile stresses at the top flange/lip junction, which oppose the compression stresses due to major axis bending moment. This results in increasing the compression stresses at the top half of the web and a portion of the top flange. However, the other portion of the top flange is in tension. This effectively anchors the top flange against distortional buckling, however reduces the local buckling critical stress in the web.

The dominant failure mode observed experimentally for CFS bolted moment connections is characterized by buckling of the web close to the connection zone, first reported by Kirk (1986). Experimental work on apex connections showed that the strength of the connections can be also influenced by lateral-torsional buckling of the gusset plate (Öztürk and Pul, 2015). In other relevant studies, Chung and Lau (1999) and Wong and Chung (2002) investigated experimentally the structural performance of the CFS bolted moment connections. Using perpendicular springs for modelling of the bolts, Lim and Nethercot (2003) showed that the bolt-group length can have a significant effect on the capacity of the CFS bolted connections under pure bending. In a follow-up study, Lim et al. (2016) demonstrated that the Direct Strength Method (DSM) (AISI S100-16, 2016) can be adequately used to find the strength of the CFS bolted-moment connections with practical connection sizes. In another study, Bučmys (2018) predicted analytically the moment-rotation behaviour of bolted-moment

connections by using a set of springs to represent gusset plate, beam bolt-group and column bolt-group. More recently, Rinchen et al. (2019a, 2019b) investigated the moment-rotation behaviour of different types of connections used in CFS portal frames including apex, eaves and base connections through experimental tests and advanced numerical modelling. The results of their study were also used to develop a practical method to design cold-formed steel single C-section portal frames using Direct Strength Method and Direct Design Method (Rinchen et al., 2019). Sabbagh et al. (2012) conducted cyclic tests to evaluate the hysteretic behaviour of CFS bolted-moment connections considering bearing and slippage of the bolts. It was shown that adding flange bends in the beam cross-section can generally improve the performance of the connection. Similarly, Ye et al. (2019b, 2019a) showed the dependency of seismic characteristics of the bolted-moment connections on the beam cross-sectional shapes and thicknesses, gusset plate thicknesses, and bolt configurations.

It should be mentioned that most of the above-mentioned analytical studies mainly focused on the global behaviour of the CFS bolted moment connections under different types of load (i.e. monotonic and cyclic) without considering the effects of bimoment. This highlights the need to develop a general design approach to predict the flexural strength of CFS bolted moment connections, which takes into account the bimoment. The influence of cross-sectional shape on increasing or decreasing the bimoment effect is another important issue which needs to be addressed. This paper aims to propose an analytical design approach using EC3 effective width method and classical structural analysis theories for determining the ultimate flexural strength of CFS bolted moment connections by taking into account the effect of bimoment. To assess the accuracy of the proposed analytical design approach, the calculated results are compared with the results of previous experimental tests as well as experimentally validated Finite Element (FE) models subjected to pure bending moment. An optimisation framework is then presented, using Genetic Algorithm (GA) linked to the proposed analytical design approach developed in

MATLAB (2015), to optimise the beam cross-sectional shapes in CFS bolted moment connection for maximum flexural capacity.

## 2 Analytical approach

### 2.1 Description of torsion and bimoment

St. Venant's theory can be applied for a member under uniform torsion, based on the fundamental assumption of plane sections after twisting. It is well-known that this assumption holds true for circular closed sections, while it may not be accurate for open sections and non-circular closed sections. The cross-sections of thin-walled CFS members in torsion generally exhibit warping, and therefore, do not remain plane (known as non-uniform torsion). For the case of channel section, if this warping is restrained, in-plane bending moment will be generated in the flange, but in the opposite direction in each flange. Vlasov (1961) initially investigated this type of behaviour using classical structural theories and defined the induced bending in the flanges caused by warping restraint as bimoment. The presence of bimoment leads to normal stresses in the cross-section, which act similar to the flexural stresses and may be of the same order of magnitude. In this section, the warping torsion formulations are developed for bolted moment connections with CFS lipped-channel section to take into account the effect of the bimoment. The principle of superposition is then used to combine the longitudinal stresses due to bending and warping.

In non-uniform torsion, in addition to the St. Venant shear stresses, longitudinal strains are also present owing to the warping. Consequently, normal longitudinal stresses are generated at the cross-section, which vary along the member length. It should be noted that the generated longitudinal stresses caused by warping are directly related to the level of resistance against warping. The applied torsional moment  $T$  is divided into two terms: (I) a torsion as a result of the uniform torsional rotation of the cross-section ( $T_t$ ), and (II) a warping torsion caused by the warping restraint ( $T_w$ ):

$$T = T_t + T_w$$

(1)

For the case of uniform torsion, the angle of rotation per unit length ( $\frac{d\phi}{dx}$ ) is proportional to the torsional moment ( $T_t$ ):

$$\frac{d\phi}{dx} = \frac{T_t}{GI_t}$$

(2)

where  $I_t$  is the torsion constant;  $G$  is the shear modulus;  $\phi$  is the twist of the section;  $x$  is the length variable coinciding the longitudinal axis of the member. By considering the bending of the flanges due to warping, the second term of the applied torsional moment,  $T_w$ , for the torsion of a non-circular section is then expressed by:

$$T_w = -EI_w \frac{d^3\phi}{dx^3}$$

(3)

where  $E$  is the elastic section modulus, and  $I_w$  is the warping constant. The longitudinal stresses and shear stresses due to an applied torsional moment ( $T$ ) can be evaluated using the solution of the Eq. (1) with appropriate boundary conditions. By differentiating the equation for the torsion of a non-circular section:

$$\frac{dT}{dx} = -EI_w \frac{d^4\phi}{dx^4} + GI_t \frac{d^2\phi}{dx^2} = -m$$

(4)

or

$$\frac{d^4\phi}{dx^4} - k^2 \frac{d^2\phi}{dx^2} = \frac{m}{EI_w}$$

(5)

where  $k = \sqrt{\frac{GI_t}{EI_w}}$  and  $m$  denotes the intensity of a distributed torsional moment ( $m=0$  for a concentrated torsional moment). The general solution of Eq. (5) is as follow:

$$\phi = C_1 \cosh kx + C_2 \sinh kx + C_3 x + C_4 + \phi_0$$

(6)

where  $\phi_0$  is a particular solution and is taken:  $\phi_0=0$  for  $m=0$  and  $\phi_0 = \frac{mx^2}{2GI_t}$  for uniform  $m$ .  $C_1$  to  $C_4$  are constants which should be solved based on the boundary conditions of the CFS bolted moment connection (see Fig. 2). In general, in this study four different restrictions are imposed on the beam cross-section subjected to bimoment (warping torsion):

(1) Twist of the section at  $x= 0$  and  $L$  is prevented.

$$\phi = 0$$

(7)

(2) Warping of the cross-section plane at  $x= 0$  and  $L$  is prevented.

$$\frac{d\phi}{dx} = 0$$

(8)

(3) The known external torsional moment is  $T_0$  at one end of the beam ( $x= 0$ ).

$$T = T_t + T_w = -EI_w \frac{d^3\phi}{dx^3} + GI_t \frac{d\phi}{dx} = T_0$$

(9)



(4) The bimoment ( $B$ ) is externally applied ( $B_0$ ) at one end of the beam ( $x= 0$ ).

$$B = -EI_w \frac{d^2 \phi}{dx^2} = B_0$$

(10)

## 2.2 Development of bimoment in CFS bolted moment connection

A typical CFS bolted-moment connection is generally formed through a plate bolted to the webs of the CFS back-to-back channel sections. The strength of the CFS sections at the joint is mainly determined based on the distribution of internal bolt-forces ( $f_i$ ) (Blum and Rasmussen, 2019). Fig. 2 shows the internal bolt-forces ( $f_i$ ) of a typical bolt-group (formed from nine bolts with the length of  $a_b$  and the height of  $b_b$ ) used in a connection under pure bending. The bolt-group resists against an applied bending moment ( $M_{c.r}$ ) and rotates about a point known as the centre of rotation (c.r). Therefore, each internal bolt force ( $f_i$ ) acts in a direction perpendicular to the line drawn from the centre of rotation to the bolt-hole, while it is proportional to its distance  $d_i$  from the centre of rotation:

$$f_i = c d_i$$

(11)

where  $c$  is a constant calculated based on the equilibrium of applied bending moment and internal bolt forces using the following equations:

$$c = \frac{M_{c.r}}{\sum_{i=1}^n d_i^2}$$

(12)

$$M_{c.r} = \sum_{i=1}^n f_i d_i$$

(13)

where  $n$  is the number of bolts in the bolt-group. It is worth mentioning that, for a connection under pure bending moment, the bolt-group centre of rotation (c.r) coincides with the centre of the bolt-group (c.b), as shown in Fig. 2. In general, the web of each channel section in the CFS bolted connection under pure bending moment at the right end is subjected to the forces acting through bolt-group (see Fig. 2). Based on a free body diagram of the segment between sections a-a and b-b cutting through the first column of the bolt-group and the location of warping restraint, the shear force on section a-a acting upwards has a magnitude of:

$$V = V_a = 2f_{1y} + f_2 = \frac{M_b a_b}{a_b^2 + b_b^2}$$

(14)

where  $M_b$  is the applied bending moment at section b-b, which is assumed to be equal to the moment transferred to the centre of rotation  $M_{c.r}$ .  $a_b$  and  $b_b$  represent the length and the height of the bolt-group, respectively (see Fig. 2).

The diagram of shear flow distribution generated by the shear force ( $V$ ) on a CFS lipped-channel section is shown in Fig. 3. Due to eccentricity of the bolt-group forces from the shear centre of section ( $e$ ), clockwise twisting moment ( $T$ ) is then applied on the cross-section:

$$T = V.e$$

(15)

To develop an equation for the bimoment induced in CFS bolted moment connections, the constants  $C_1$  to  $C_4$  in general Eq. 6 for the twist of the section first need to be specified. Four different general restrictions proposed in section 2.1 are applied at sections a-a and b-b (see Fig. 2) to calculate the values of these constants parameters:

Cross-section a-a:

$$\begin{cases} \left(\frac{d\phi}{dx}\right)_{x=0} = 0 \\ GI_t \left(\frac{d\phi}{dx}\right)_{x=0} - EI_w \left(\frac{d^3\phi}{dx^3}\right)_{x=0} = T \end{cases} \quad \text{and,}$$

(16)

$$\begin{cases} kC_2 + C_3 = 0 \\ k^3 C_2 = -T/EI_w \end{cases}$$

(17)

Cross-section b-b:

$$\begin{cases} \left(\frac{d\phi}{dx}\right)_{x=L} = 0 \\ GI_t \left(\frac{d\phi}{dx}\right)_{x=L} - EI_w \left(\frac{d^3\phi}{dx^3}\right)_{x=L} = T \end{cases} \quad \text{and,}$$

(18)

$$\begin{cases} kC_1 \sinh(kL) + kC_2 \cosh(kL) + C_3 = 0 \\ k^3 C_1 \sinh(kL) + k^3 C_2 \cosh(kL) = -T/EI_w \end{cases}$$

(19)

where  $L$  is the distance between a-a section ( $x = 0$ ) and b-b section ( $x = L$ ). It should be noted that warping is assumed to be fully restrained (i.e.  $\frac{d\phi}{dx} = 0$ ) in this study, leading to generate a bimoment on the cross-section. The value of bimoment ( $B$ ) at cross-section a-a ( $x = 0$ ) is then calculated using following equation:

$$B = -EI_w \frac{d^2\phi}{dx^2} = -EI_w k^2 C_1$$

(20)

where  $C_1$  is obtained from the Eqs. 17 and 19:

$$C_1 = \left(-\frac{T}{k^3 EI_w}\right) \left(\frac{1 - \cosh(kL)}{\sinh(kL)}\right)$$

(21)

The longitudinal stress  $\sigma_B$  associated with a bimoment ( $B$ ) is directly calculated based on the gross properties using the following equation:

$$\sigma_B = \frac{B\omega}{I_w}$$

(22)

where  $\omega$  is the sectorial coordinate which varies around the section, as shown in Fig. 4.

In this study, the longitudinal stress caused by bending moment ( $\sigma_M$ ) is calculated based on the Eurocode 3 (EC3) effective width method (CEN, 2005, CEN, 2006) using the effective properties of the cross-section. The effect of local buckling is taken into account in accordance with EC3 effective width method, in which the load-bearing stresses shift toward the corner zones by reducing the effective width of the constituent plates to reflect the fact that the flat portions of the cross-section contribute less to the load-bearing capacity. The distortional buckling (or flexural–torsional buckling of plate sub-assemblies) is also considered based on EC 3 by applying a reduction factor on the effective plate thickness of each sub-assembly.

Therefore, the total longitudinal stress ( $\sigma_t$ ) applied on the CFS cross-section is calculated using superposition of the flexural and bimoment longitudinal stresses:

$$\sigma_t = \sigma_M + \sigma_B = \frac{M_b}{I_{eff}} y_{eff} + \frac{B}{I_w} \quad (\sigma_t \leq f_y)$$

(23)

where  $I_{eff}$  is the effective second moment of area of the cross-section, and  $y_{eff}$  denotes the effective distance from centroid of the cross-section to the critical buckling point. The maximum capacity of the

connection ( $M_{Bi}$ ) is achieved when the total longitudinal stress ( $\sigma_t$ ) reaches the yield strength of the CFS beam cross-section ( $f_y$ ). Previous experimental studies reported that the dominant failure mode is the local buckling of the web near connection zone, where the farthest bolt from the centre of rotation is located (Lim and Nethercot, 2003). In this study, the critical buckling point is assumed to be immediately after the farthest bolt-hole line ( $1.5d_b$  away from the bolt centre line), where  $d_b$  is the diameter of the bolt (see Fig. 5).

### 3 Accuracy of the proposed analytical approach

#### 3.1 Comparison with experimental tests results

In this section, the accuracy of the proposed analytical approach for the connections under pure bending is assessed based on the results of the experimental tests on the CFS apex joints conducted by Lim and Nethercot (2003). Four apex joints with different bolt-group length were tested under four-point bending (see Fig. 6). All bolt-groups consisted of an array of nine bolts, and the nominal diameter of the bolts was 16 mm. A back-to-back CFS lipped-channel section was used with the dimensions shown in Fig. 6. The modulus of elasticity ( $E$ ) and the yield capacity ( $f_y$ ) were 210 GPa, and 358 MPa, respectively, determined based on the average of three tensile coupon test results. The maximum distance between the points of lateral restraint around the apex joint was 1036 mm. The length of the segment between sections a-a and b-b for the tested apex connections (see Fig. 6) are listed in Table 1. It should be noted that the dominant failure mode was local buckling of the webs of the channel sections (see Fig. 7), and no buckling of the apex brackets was observed in the experiments. This is consistent with the initial assumption made to develop the analytical approach (see section 2).

The results of the tested apex connections based on the proposed analytical approach are listed in Table 2. It is shown that there is a very good agreement between the capacities of the connections under pure

bending predicted by the analytical model ( $M_{Bi}$ ) and those obtained from experimental tests ( $M_{Bi}^{exp}$ ) with on average less than 3% error (COV of 0.04). This implies that the CFS bolted moment connection under pure bending can be designed for the full effect of bimoment. Similar to the experimental results, it is shown in Table 2 that increasing the bolt-group length ( $a_b$ ) could significantly decrease the bimoment ( $B$ ) and consequently enhance the connection strength ( $M_{Bi}$ ). The proposed analytical approach is also compared with the results of DSM developed by Lim et al. (2016) to estimate the capacity of the CFS bolted moment connections ( $M_{Bi}^{DSM}$ ). It is seen that the predicted capacities based on DSM approach are not very accurate for the longest and the shortest bolt-group lengths (around 15% error).

In general, the negative effect of the bolts on the capacity of CFS section is seen by comparing the ratios of the connection strength ( $M_{Bi}^{exp}$ ) to the capacity of the back-to-back channel section calculated based on the EC3 effective width method ( $M_{M,EC3}$ ). It can be seen that the accuracy of the EC3 predictions was considerably lower (up to 19% error) for the connections with shorter bolt-group length due to the bimoment effects as discussed before.

It is worth mentioning that while it is more accurate to consider the back-to-back channel as a built-up section (Meza et al., 2019), in this study, the buckling resistance of the connection with back-to-back channel section is calculated based on the assumption that single channels can buckle individually. This approach leads to conservative design solutions and has been previously used by other researchers (e.g. (Ye et al., 2018c, Ye et al., 2018b)).

### **3.2 Comparison with Finite Element (FE) analysis results**

FE modelling has previously been used to predict the behaviour of CFS bolted connections with gusset plates (Lim and Nethercot, 2004b, Sabbagh et al., 2013, Elkersh, 2010, Serror et al., 2016, Öztürk and Pul, 2015) and good agreement between the test results and the FE predictions has generally been reported. In this study, the ABAQUS software (2014) is used to create detailed FE models of the apex

connections tested by Lim and Nethercot (2003), accounting for material nonlinearity, geometric imperfections and accurate bolt bearing behaviour. The validated models are then expanded to investigate the accuracy of the proposed analytical approach discussed in section 2.

### **3.2.1 Bolt modelling**

To accurately model the bearing behaviour of the bolts, “discrete fastener” elements available from the ABAQUS library (2014) are adopted. For the purpose of validating the FE model, the bearing behaviour of the bolt against the channel web is obtained from a lap shear test conducted by Lim and Nethercot (2004a). In the adopted modelling approach, the displacement and rotation of each fastening point are coupled to the average rotation and displacement of the surface nodes within a radius of influence. While it is recommended in the ABAQUS manual (2014) to consider the radius of influence equal to the radius of the bolt shank, a sensitivity analysis performed as part of this study showed that this parameter had a negligible effect on the behaviour of the connections, mainly because bolt failure was not critical.

### **3.2.2 Element type, material properties and boundary conditions**

The general-purpose S4R element, which is a 4-noded quadrilateral shell element with reduced integration, is selected to model both the CFS beam and the gusset plate in this study. Following a mesh sensitivity analysis, a mesh size of  $10 \times 10 \text{ mm}^2$  is considered to provide a balance between accuracy and computational cost. A bi-linear material stress-strain model is used with an elastic modulus  $E = 210 \text{ GPa}$ , followed by a linear hardening range with a slope of  $E/100$ . This slope is obtained according to the coupon tests results presented in Lim and Nethercot (2003). The yield stress and the ultimate stress measured from the coupon tests are:  $f_y=358 \text{ MPa}$  and  $f_u=425 \text{ MPa}$  for the channel sections, and  $f_y=341 \text{ MPa}$  and  $f_u=511 \text{ MPa}$  for the gusset plate.

The geometry and the boundary conditions of the developed FE model are shown in Fig. 8. The nodes belonging to each end section are first coupled to the centroid of the whole cross-section, where a reference point is defined. Simply supported boundary conditions are then applied to the reference point at both ends, as clarified in Fig. 8. The lateral displacements of the webs are prevented at the locations of the bolts similar to the experimental test setup. Finally, point loads are applied in a displacement control manner to the reference points, which are coupled to all the nodes of the cross-section at the load application points.

### **3.2.3 Geometric imperfections**

It is assumed in this study that the global failure of the CFS beam due to lateral-torsional buckling is prevented by a lateral bracing system similar to the experimental test setup (Lim and Nethercot, 2003). Therefore, only local and distortional imperfections are considered in the developed models, depending on which mode has lower critical buckling stress. An elastic buckling analysis in ABAQUS is conducted to generate the geometric imperfections by using a scaled first mode shape. Based on the work by Schafer and Peköz (1998), applicable to cross-sections with less than 3 mm thickness ( $t$ ), the 50% value of the Cumulative Distribution Function of the imperfections is utilized, which scaled to amplitudes of  $0.94t$  and  $0.34t$  for the distortional and local imperfections, respectively. When the thickness of the cross-section is larger than 3mm, the imperfection magnitude is determined based on the equation proposed by Walker (1975).

### **3.2.4 Verification and sensitivity study**

The FE model is verified against the four aforementioned full-scale tests on bolted CFS apex connections (Lim and Nethercot, 2003). The FE predicted capacities  $M_{Bi}^{FE}$  are compared to the experimentally obtained capacities  $M_{Bi}^{exp}$  in Table 2. In general, a good agreement is obtained with an average ratio of  $M_{Bi}^{exp} / M_{Bi}^{FE}$  of 0.99 and a COV of 0.02. Subsequently, a sensitivity study is performed to assess the



accuracy of the proposed analytical design approach using the validated FE models of the connections with a wide range of CFS cross-sections, as illustrated in Fig. 9. It should be noted that in the proposed analytical approach, it was assumed that warping is fully restrained. However, in the studied connections the flanges are not directly connected and the warping is restrained in the beam webs by the connection bolts. This implies that the assumption of fully restrained warping would be only acceptable for the sections with higher warping constant ( $I_w$ ). The results in Fig. 9 confirm that the proposed analytical approach can be reasonably used when the warping constant ( $I_w$ ) of the beam cross-section is larger than  $10^{10} \text{ mm}^6$ . The maximum error in the estimated capacity of the connections in this case was less than 15%, which is considered to be acceptable for practical design applications. As expected, it is shown that the accuracy of the proposed method is considerably improved for the sections with higher warping constant parameter.

To provide reliable design solutions in this study, it was checked that the values of warping constant of all CFS beam sections were in the acceptable range (i.e.  $I_w > 10^{10} \text{ mm}^6$ ). However, further studies are required to develop a more accurate analytical approach for the CFS sections with lower  $I_w$  values.

#### **4 Definition of optimisation problems**

This section is aimed to optimise the flexural capacity of CFS bolted moment connections by taking into account the effects of bimoment determined according to the proposed analytical approach (see section 2) through changing the cross-sectional dimensions of the beam members. The CFS lipped-channel cross-section with the same dimensions (336×88×20 mm) and material properties ( $E= 210 \text{ GPa}$ ,  $f_y=358 \text{ MPa}$ ) as the reference experimental tests was taken as a benchmark for the optimisation process (Lim and Nethercot, 2003). The total coil width of the benchmark section ( $P = 552 \text{ mm}$ ) was kept constant in the optimisation process to ensure the same amount of material is used for all sections. In this study, an additional check was also placed to ensure the warping constant ( $I_w$ ) of the beam cross-sections is larger

than  $10^{10} \text{ mm}^6$  (see Section 3.2.4). To examine the efficiency of the optimisation framework on different configurations of the CFS bolted moment connection, three different bolt-group length  $a_b/h = 1, 2$  and  $3$  and two different beam length  $L = 2h$  and  $4h$  (segment between sections a-a and b-b) are selected in this study. Three different plate thicknesses were also utilised  $t = 1, 2,$  and  $3$  mm. The optimisation target was to maximise the flexural strength of CFS sections in bolted moment connection ( $M_{Bi}$ ) providing that the stress at the critical point of the cross-section ( $1.5 d_b$  away from farthest bolt) does not exceed the yield stress:

$$\text{Max: } f(x) = M_{Bi}$$

(24)

$$\text{Subjected to: } \sigma_t \leq f_y$$

(25)

Fig. 10 shows a flowchart of the adopted optimisation process. To ensure that the optimum results satisfy all the design and practical requirements, the following constraints are imposed (see Fig. 11):

- a) The CFS beam sections were restricted to be lipped-channel as widely used in common practice.
- b) To provide enough space for roofing system connections using screws, the minimum beam flange width was considered to be 50 mm.
- c) The minimum lip length was set to be 10 mm to help the cold roll forming process of the CFS sections as suggested by the industrial advisor of the project.
- d) The minimum and maximum depth of the channel sections was considered to be 100 mm and 400 mm, respectively.

- e) All the EC3 limitations for plate slenderness (width-to-thickness ratio) and lips' angle were considered as optimisation constraints (see Fig. 11).

## 5 Real-Coded Genetic Algorithm

Conventional Genetic Algorithm (GA) has been extensively used to find the best design solutions for different types of structural components and connections (Bel Hadj Ali et al., 2009, Ramires et al., 2012, Alberdi et al., 2015). In this study, a Real-Coded Genetic Algorithm (RC-GA) (Pathan et al., 2018) was adopted to obtain CFS bolted moment connections with maximum ultimate load-bearing capacity (see Eq. 26) by satisfying all the design constraints listed in Fig. 11. Compared to conventional binary GA methods, the main advantage of RC-GA is directly applying the design variables without requiring coding and decoding. This can considerably increase the computational efficiency of the optimisation process (Lwin et al., 2014). In the adopted method, an initial population is randomly generated and then evolved through simulated binary crossover (SBX) and polynomial mutation generic operations and by utilising binary tournament selection method (Deb, 2001, Lwin et al., 2014). The random binary tournament selection is used to ensure the best solutions do not dominate the mating pool. A niching technique is also employed for selection and crossover operators to maintain the diversity of population during the optimisation process. The details of the adopted optimisation process can be found in Phan et al. (2013). A penalty approach method is used to take into account the selected design constraints (Pezeshk et al., 2000, Yeniay, 2005). To provide a better convergence, the penalty value corresponding to each violated design constraint is gradually decreased by increasing the number of generations,  $Gen$ , using the following equation (Erbatur et al., 2000):

$$CVP_i = \frac{qg_i}{Gen^{0.5}}$$

(26)

where  $CVP_i$  is the violated penalty for the  $i^{\text{th}}$  design constraint,  $g_i$  is the violated constraint, and  $q$  is a scale factor. Considering that all design constraints are unity normalised, the scale factor of 100 is used for scaling the penalty values to the same order of the objective function of the optimisation. The fitness function ( $F$ ) is defined by:

$$F = W(1 + \sum_1^u CVP_i)$$

(27)

where  $u$  represents the number of design constraints. For each solution, the fitness function is calculated based on the objective function using the penalty values corresponding to the violated constraints.

Since better solutions receive smaller fitness values, they are favourably chosen by the tournament selection operator. This leads to the lightest design solution, which satisfies all the defined design constraints. The terminating criterion in this study is to reach a predefined total number of generations.

The above-mentioned design procedure in Section 4 and the RC-GA method were implemented in Matlab (2015) to carry out the optimisation process. The GA population size and the maximum number of GA generations (i.e. termination criterion) were considered to be 50 and 100, respectively. Based on the results of a sensitivity analysis, the following GA parameters were also found to be suitable: mutation probability  $p_m = 0.01$ ; crossover probability  $p_c = 0.9$ ; niching radius = 0.25; and distribution coefficient for crossover and mutation operators = 1.0.

## 6 Optimisation results and discussions

The optimisation framework adopted in this study consists of two distinct pieces of software developed in Matlab (2015): (i) a programme implementing the proposed analytical approach, and (ii) a programme carrying out the GA (as discussed in Section 5). For each CFS bolted moment connections, the optimisation process was repeated five times using different sets of random initial populations, and the design solution with the maximum bending capacity was considered as the optimum section. In all cases, the final optimum solution was obtained with a reasonably small standard deviation.

### 6.1.1 Optimisation of tested cross-section

Using the proposed optimisation framework, the tested bolted moment connections (Tests A-D) (Lim and Nethercot, 2003) are first optimised. Fig. 12 lists the dimensions of the optimum sections and the strength improvements compared to the tested specimens for different bolt-group lengths. It should be noted that at this stage the lips' angle is kept perpendicular to the flanges ( $\theta=90^\circ$ ) during the optimisation process. While the optimum cross-sections generally tend to provide the minimum specified flange width, decreasing the bolt-group length (i.e. increasing the bimoment) leads to an increase in the web height and consequently a decrease in the lip length. It can be seen that by simply optimising the relative dimensions of the lipped-channel section without considering the effect of bimoment, the capacity of the cross-section ( $M_{M,EC3}$ ) is slightly (up to 9%) increased. However, the results of optimisation considering the effect of bimoment indicate that the optimisation process possesses the highest level of efficiency in terms of strength ( $M_{Bi}$ ) by up to 24% for the connections with short bolt-group length where the largest amount of bimoment exists (Test A). As expected, the effect of bimoment on the efficiency of the optimisation process and the optimum design solution was less prominent (up to 10%) for the connections with larger bolt-group length (Test D). To assess the accuracy of the proposed analytical approach for the optimised sections, FE models of connections with

optimised beam sections are developed and the results of flexural capacities ( $M_{Bi}^{FE}$ ) are compared with those obtained from the analytical approach ( $M_{Bi}$ ). As shown in Fig. 12, the proposed analytical approach could reasonably predict the flexural capacity of the optimum design connections with less than 11% error (average error of 7%).

### **6.1.2 Effects of beam length and plate thickness on the optimum solutions**

In this section, the typical CFS bolted moment connections are optimised by taking into account different beam lengths ( $L$ ), bolt-group lengths ( $a_b/h$ ), and plate thicknesses ( $t$ ). The calculated cross-sectional dimensions, properties and flexural capacity of the tested and optimised CFS bolted moment connections are listed in Tables 3 and 4, respectively. While using larger bolt-group length in the connection in general generates a smaller bimoment on the beam cross-section, it is shown that increasing the beam length and plate thickness leads to an increase in the value of the bimoment ( $B$ ) (see Tables 3 and 4). As shown in Table 4, optimum solutions always provide the minimum specified flange width ( $b=50$  mm), regardless of the beam length and plate thickness. The results also demonstrate that the variation of either the beam length or the plate thickness generally results in slight changes in the lips' length (or web height) of the optimum sections. It can be seen that, for the given plate thickness and width, the proposed optimisation method could significantly increase (up to 36%) the maximum flexural capacity of the CFS bolted moment connections ( $M_{Bi}$ ) compared to the benchmark tested connections ( $M_{Bis}$ ). It is also observed that the optimisation process is more efficient for the bolted moment connections with smaller bolt-group length ( $a_b/h$ ) and larger beam length ( $L$ ). To investigate the negative effect of bimoment on the capacity of CFS sections, the ratio of the connection strength ( $M_{Bi}^{exp}$ ) to the capacity of the adopted beam sections (i.e. back-to-back channel) determined based on the EC3 ( $M_{M,EC3}$ ) is calculated for different design parameters (i.e.  $a_b/h$ ,  $t$  and  $L$ ). Fig. 13 (a) and (b) compare the results of the standard and optimised cross-sections, respectively. It can be seen that

the presence of the bolts could considerably reduce the capacity of the cross-sections, especially for shorter bolt-group lengths (up to 44% for the connection with  $L=4h$  and  $t=3$  mm). However, the effect of bimoment is generally mitigated by using longer bolt-group length, lower beam length and thinner plates (see Fig. 13).

The accuracy of the adopted design method is also assessed by a comparison between the flexural capacities of the connections calculated using the proposed analytical approach and those obtained from detailed FE models. The results in Table 3 indicate that the proposed analytical approach could predict the capacity of the connections with less than 8% error on average.

## 7 Summary and conclusions

This paper presented an alternative analytical design approach using Eurocode 3 (EC3) effective width method to predict the ultimate bending capacity of CFS bolted moment connections by considering bimoment effects. The predicted capacities based on the analytical approach were first compared with the results of experimental tests on CFS apex connections. It was demonstrated that decreasing bolt-group length can significantly increase the effect of bimoment and consequently reduce the connection strength. Experimentally validated FE models were then developed by taking into account geometrical imperfections and material nonlinearity to assess the accuracy of the analytical approach for a wide range of cross-section dimensions. It was shown that the proposed approach is adequate to predict the capacity of the bolted moment connections with cross-sections with warping constants ( $I_w$ ) over  $10^{10}$  mm<sup>6</sup>. Subsequently, the proposed analytical approach was combined with an optimisation framework using a Real-Coded Genetic Algorithm (RC-GA) to mitigate the effect of bimoment by optimising the cross-sectional shape of the CFS beam elements. To provide practical design solutions, the EC3 design limits, as well as a number of manufacturing and end-use constraints, were taken into account in the optimisation process. In general, the presence of the bolts could significantly (up to 44%) reduce the

capacity of the cross-sections, especially for shorter bolt-group lengths. However, it was shown that the effect of bimoment could be mitigated by longer bolt-group length, lower beam length and thinner plates. As a general trend, optimum cross-sections always adopted the minimum specified flange width regardless of the beam length, plate thickness, and bolt-group length. However, decreasing the bolt-group length (i.e. increasing the bimoment) led to an increase in the web height and consequently a decrease in the lip length of the optimum cross-sections. The results also showed that the variation of the beam length and the plate thickness generally resulted in slight changes in the lips' length (or web height) of the optimum sections. Using the same plate width and thickness, the proposed optimisation method could significantly (up to 36%) increase the flexural strength of the CFS bolted moment connection compared to the benchmark tested connections, while the optimisation process was more efficient for the bolted moment connections with smaller bolt-group length and larger beam length. The results of this study should prove useful for more efficient design of CFS sections in bolted moment connections considering bimoment.

### **Data Availability Statement**

Some or all data, models, or code generated or used during the study are available from the corresponding author by request. Material properties data, geometric imperfections data, connector behaviour data, and optimisation data.

### **Acknowledgement**

This research was supported by the Engineering and Physical Sciences Research Council (EPSRC) grants EP/L019116/1. The second author was also supported by EPSRC Doctoral Scholarship grant 1625179.

### **References**

Abaqus/CAE User's Manual (2014). "version 6.14-2, USA".  
AISI S100-16 (2016). "North American specification for the design of cold-formed steel structural members. ". *American Iron and Steel Institute (AISI), Washington, DC, USA.*



- Alberdi, R., Murren, P. and Khandelwal, K. (2015). "Connection topology optimization of steel moment frames using metaheuristic algorithms". *Engineering Structures*, 100, 276-292.
- Bagheri Sabbagh, A., Petkovski, M., Pilakoutas, K. and Mirghaderi, R. (2012). "Experimental work on cold-formed steel elements for earthquake resilient moment frame buildings". *Engineering Structures*, 42, 371-386.
- Bel Hadj Ali, N., Sellami, M., Cutting-Decelle, A.-F. and Mangin, J.-C. (2009). "Multi-stage production cost optimization of semi-rigid steel frames using genetic algorithms". *Engineering Structures*, 31, 2766-2778.
- Blum, H. B. and Rasmussen, K. J. R. (2019). "Experimental investigation of long-span cold-formed steel double channel portal frames". *Journal of Constructional Steel Research*, 155, 316-330.
- Bučmys, Ž., Daniūnas, A., Jaspert, J.-P. and Demonceau, J.-F. (2018). "A component method for cold-formed steel beam-to-column bolted gusset plate joints". *Thin-Walled Structures*, 123, 520-527.
- CEN (2005). "Eurocode 3: design of steel structures, part 1.3: general rules—supplementary rules for cold formed members and sheeting, in, Brussels: European Committee for Standardization".
- CEN (2006). "Eurocode 3: Design of steel structures, Part 1-5: Plated structural elements, in, Brussels: European Committee for Standardization".
- Chung, K. F. and Lau, L. (1999). "Experimental investigation on bolted moment connections among cold formed steel members". *Engineering Structures*, 21, 898-911.
- Deb, K. (2001). "Multi-objective optimization using evolutionary algorithms. Chichester: John Wiley and Sons, Inc."
- Dubina, D., Stratan, A. and Nagy, Z. (2009). "Full-scale tests on cold-formed steel pitched-roof portal frames with bolted joints". *Advanced Steel Construction*, 5, 175-194.
- Elkersh, I. (2010). "Experimental investigation of bolted cold formed steel frame apex connections under pure moment". *Ain Shams Engineering Journal*, 1, 11-20.
- Erbatur, F., Hasaḇebi, O., Tütüncü, İ. and Kılıç, H. (2000). "Optimal design of planar and space structures with genetic algorithms". *Computers & Structures*, 75, 209-224.
- Kirk, P. (1986). "Design of a cold-formed section portal frame building system". *Proc. 8th International Speciality Conference on Cold-formed Steel Structures, St. Louis, MO, University of Missouri-Rolla; p.295.*
- Lim, J. B. P., Hancock, G. J., Clifton, G. C., Pham, C. H. and Das, R. (2016). "DSM for ultimate strength of bolted moment-connections between cold-formed steel channel members". *Journal of Constructional Steel Research*, 117, 196-203.
- Lim, J. B. P. and Nethercot, D. A. (2003). "Ultimate strength of bolted moment-connections between cold-formed steel members". *Thin Wall Structures*, 41, 1019-1039.
- Lim, J. B. P. and Nethercot, D. A. (2004a). "Finite element idealization of a cold-formed steel portal frame". *Journal of Structural Engineering*, 130, 78-94.
- Lim, J. B. P. and Nethercot, D. A. (2004b). "Stiffness prediction for bolted moment-connections between cold-formed steel members". *Journal of Constructional Steel Research*, 60, 85-107.
- Lwin, K., Qu, R. and Kendall, G. (2014). "A learning-guided multi-objective evolutionary algorithm for constrained portfolio optimization". *Applied Soft Computing*, 24, 757-772.
- Mathworks (2015). "Matlab R2015b". *Mathworks Inc.*
- Meza, F. J., Becque, J. and Hajirasouliha, I. (2019). "Experimental study of cold-formed steel built-up columns". *Thin-Walled Structures (in press)*.
- Mojtabaei, S. M., Kabir, M. Z., Hajirasouliha, I. and Kargar, M. (2018). "Analytical and experimental study on the seismic performance of cold-formed steel frames". *Journal of Constructional Steel Research*, 143, 18-31.

- Mojtabaei, S. M., Ye, J. and Hajirasouliha, I. (2019). "Development of optimum cold-formed steel beams for serviceability and ultimate limit states using Big Bang-Big Crunch optimisation". *Engineering Structures*, 195, 172-181.
- Öztürk, F. and Pul, S. (2015). "Experimental and numerical study on a full scale apex connection of cold-formed steel portal frames". *Thin-Walled Structures*, 94, 79-88.
- Pathan, M. V., Patsias, S. and Tagarielli, V. L. (2018). "A real-coded genetic algorithm for optimizing the damping response of composite laminates". *Computers & Structures*, 198, 51-60.
- Pezeshk, S., Camp, C. V. and Chen, D. (2000). "Design of Nonlinear Framed Structures Using Genetic Optimization". *Journal of Structural Engineering*, 126, 382-388.
- Phan, D. T., Lim, J. B. P., Tanyimboh, T. T. and Sha, W. (2013). "An efficient genetic algorithm for the design optimization of cold-formed steel portal frame buildings". *Steel and Composite Structures, An International Journal*, 15(5), 519-538.
- Phan, D. T., Mojtabaei, S. M., Hajirasouliha, I., Ye, J. and Lim, J. B. P. (2019). "Coupled element and structural level optimisation framework for cold-formed steel frames". *Journal of Constructional Steel Research*, 105867.
- Ramires, F. B., Andrade, S. A. L. d., Vellasco, P. C. G. d. S. and Lima, L. R. O. d. (2012). "Genetic algorithm optimization of composite and steel endplate semi-rigid joints". *Engineering Structures*, 45, 177-191.
- Rinchen and Rasmussen, K. J. R. (2019a). "Behaviour and modelling of connections in cold-formed steel single C-section portal frames". *Thin-Walled Structures*, 143, 106233.
- Rinchen and Rasmussen, K. J. R. (2019b). "Numerical modelling of cold-formed steel single C-section portal frames". *Journal of Constructional Steel Research*, 158, 143-155.
- Rinchen, Rasmussen, K. J. R. and Zhang, H. (2019). "Design of cold-formed steel single C-section portal frames". *Journal of Constructional Steel Research*, 162, 105722.
- Sabbagh, A. B., Mirghaderi, R., Petkovski, M. and Pilakoutas, K. (2010). "An integrated thin-walled steel skeleton structure (two full scale tests)". *Journal of Constructional Steel Research*, 66, 470-479.
- Sabbagh, A. B., Petkovski, M., Pilakoutas, K. and Mirghaderi, R. (2013). "Cyclic behaviour of bolted cold-formed steel moment connections: FE modelling including slip". *Journal of Constructional Steel Research*, 80, 100-108.
- Schafer, B. W. (2006). "CUFSM Version 3.12". *Department of Civil Engineering, Johns Hopkins University*, <http://www.ce.jhu.edu/bschafer/cufsm/>.
- Schafer, B. W. and Peköz, T. (1998). "Computational modeling of cold-formed steel: characterizing geometric imperfections and residual stresses". *Journal of Constructional Steel Research*, 47, 193-210.
- Serror, M. H., Hassan, E. M. and Mourad, S. A. (2016). "Experimental study on the rotation capacity of cold-formed steel beams". *Journal of Constructional Steel Research*, 121, 216-228.
- Vlasov, V. Z. (1961). "Thin-Walled Elastic Beams". *Jerusalem, Israel Program for scientific translations*.
- Walker, A. C. 1975. *Design and analysis of cold-formed sections*, Halsted Press.
- Wang, B., Bosco, G. L., Gilbert, B. P., Guan, H. and Teh, L. H. (2016). "Unconstrained shape optimisation of singly-symmetric and open cold-formed steel beams and beam-columns". *Thin-Walled Structures*, 104, 54-61.
- Wong, M. F. and Chung, K. F. (2002). "Structural behaviour of bolted moment connections in cold-formed steel beam-column sub-frames". *Journal of Constructional Steel Research*, 58, 253-274.
- Ye, J., Becque, J., Hajirasouliha, I., Mojtabaei, S. M. and Lim, J. B. P. (2018a). "Development of optimum cold-formed steel sections for maximum energy dissipation in uniaxial bending". *Engineering Structures*, 161, 55-67.
- Ye, J., Mojtabaei, S. M. and Hajirasouliha, I. (2018b). "Local-flexural interactive buckling of standard and optimised cold-formed steel columns". *Journal of Constructional Steel Research*, 144, 106-118.

- Ye, J., Mojtabaei, S. M. and Hajirasouliha, I. (2019a). "Seismic performance of cold-formed steel bolted moment connections with bolting friction-slip mechanism". *Journal of Constructional Steel Research*, 156, 122-136.
- Ye, J., Mojtabaei, S. M., Hajirasouliha, I. and Pilakoutas, K. (2019b). "Efficient design of cold-formed steel bolted-moment connections for earthquake resistant frames". *Thin-Walled Structures*.
- Ye, J., Mojtabaei, S. M., Hajirasouliha, I., Shepherd, P. and Pilakoutas, K. (2018c). "Strength and deflection behaviour of cold-formed steel back-to-back channels". *Engineering Structures*, 177, 641-654.
- Yeniay, O. (2005). "Penalty function methods for constrained optimization with genetic algorithms". *Mathematical and Computational Applications*, 10(1), 45-56.

## Nomenclature

$h$	web height
$b$	flange width
$c$	lip length
$\theta$	lip's angle
$t$	plate thickness
$P$	total coil width
$L$	beam length (segment between a-a and b-b)
$G$	shear modulus
$E$	elastic section modulus
$f_y$	material yield stress
$f_u$	material ultimate stress
$e$	shear centre of the section
$I_w$	warping constant
$I_t$	torsion constant
$\omega$	sectorial coordinate
$I_{eff}$	effective second moment of area of the cross-section
$y_{eff}$	effective distance from centroid of the cross-section to the critical buckling point
$m$	intensity of a distributed torsional moment
$C_1$ to $C_4$	constants
$x$	is the length variable coinciding the longitudinal axis of the member
$\phi$	twist of the section
$\phi_0$	particular solution
$T$	applied torsional moment
$T_t$	torsion due to the uniform torsional rotation of the cross-section
$T_w$	warping torsion caused by the warping restraint
$T_0$	external torsional moment
$B$	bimoment
$B_0$	externally applied
$M_{c,r}$	bending moment at centre of rotation
$M_b$	applied bending moment at section b-b
$M_{Bi}$	predicted flexural capacity of the connection considering bimoment based on proposed

	analytical approach
$M_{Bi,s}$	predicted flexural capacity of the connection with standard beam section considering bimoment based on proposed analytical approach
$M_{Bi}^{DSM}$	predicted flexural capacity of the connection considering bimoment based on DSM
$M_{Bi}^{FE}$	predicted flexural capacity of the connection considering bimoment based on FE
$M_{Bi,s}^{FE}$	predicted flexural capacity of the connection with standard beam section considering bimoment based on FE
$M_{Bi}^{exp}$	flexural capacity of the tested connections
$M_{M,EC3}$	flexural capacity of the back-to-back channel section calculated based on the EC3 effective width method (without considering bimoment)
$M_{M,EC3,s}$	flexural capacity of the standard back-to-back channel section calculated based on the EC3 effective width method (without considering bimoment)
$V=V_a$	shear force on section a-a acting
$\sigma_B$	longitudinal stress of the beam associated with a bimoment
$\sigma_M$	longitudinal stress caused by bending moment
$\sigma_t$	total longitudinal stress applied on the beam section
c.r	centre of rotation
c.b	centre of bolt-group
$d_i$	distance from the centre of rotation
$n$	number of bolts in the bolt-group
$d_b$	diameter of the bolt
$f_i$	internal bolt-forces
$a_b$	length of bolt-group
$b_b$	height of bolt-group
$CVP_i$	violated penalty for the $i^{th}$ design constraint
$g_i$	is the violated constraint
$q$	scale factor
$F$	fitness function
$Gen$	number of generation
$u$	number of design constraints
$p_m$	mutation probability
$p_c$	crossover probability

## List of Tables

**Table 1.** Experimental test results (Lim and Nethercot, 2003)

Test	Channel dimensions (mm)			$a_b$ (mm)	$b_b$ (mm)	$a_b/h$	$L$ (mm)	$M_{Bi}^{exp}$ (kN.m)
	$h$	$b$	$c$					
A	336	88	20	315	230	0.94	721	75.0
B	336	88	20	390	230	1.16	646	77.5
C	336	88	20	465	230	1.38	571	82.5
D	336	88	20	615	230	1.83	421	87.5

**Table 2.** Comparison between calculated capacities of the bolted-moment connections using analytical approach, DSM, FE, and EC3 with the experimental results

Test	Analytical approach									DSM	FE	EC3	Comparisons		
	$I_w$ $\times 10^{10}$ (mm <sup>6</sup> )	$I_{eff}$ $\times 10^6$ (mm <sup>4</sup> )	$\omega$ $\times 10^3$ (mm <sup>2</sup> )	$V$ (kN)	$T$ (kN.m)	$B$ (kN.m <sup>2</sup> )	$\sigma_B$ (MPa)	$\sigma_M$ (MPa)	$M_{Bi}$ (kN.m)	$M_{Bi}^{DSM}$ (kN.m)	$M_{Bi}^{FE}$ (kN.m)	$M_{M,EC3}$ (kN.m)	$M_{Bi}^{exp}/M_{Bi}$	$M_{Bi}^{exp}/M_{Bi}^{FE}$	$M_{Bi}^{exp}/M_{M,EC3}$
A	2.93	23.36	4.6	72.89	2.41	857.85	136.59	221.41	69.66	78.44	76.01	92.38	1.08	0.99	0.81
B	2.93	23.36	4.6	71.61	2.36	761.84	121.30	236.70	74.46		80.72		1.04	0.96	0.84
C	2.93	23.36	4.6	69.73	2.30	656.04	104.46	253.54	79.76		82.50		1.03	1.00	0.89
D	2.93	23.36	4.6	64.86	2.14	450.29	70.70	286.3	90.06		88.02		0.97	0.99	0.95
Mean												1.03	0.99	0.87	
COV												0.04	0.02	0.07	

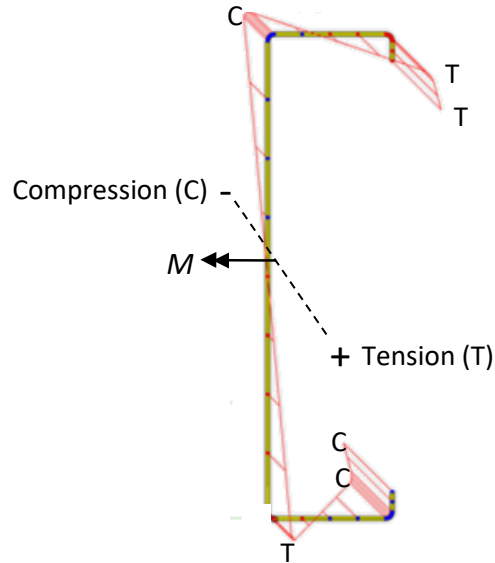
**Table 3.** Calculated properties and flexural capacity of the CFS bolted moment connections with the tested beam cross-sectional dimensions (336×88×20 mm) subject to bending at the beam end section

$a_b/h$	$t$ (mm)	$L$	$I_{eff}$ $\times 10^6$ (mm <sup>4</sup> )	$\omega$ $\times 10^3$ (mm <sup>2</sup> )	$V$ (kN)	$T$ (kN.m)	$B$ (kN.m <sup>2</sup> )	$\sigma_B$ (MPa)	$\sigma_M$ (Mpa)	$M_{Bi,s}$ (kN.m)	$M_{M,EC3,s}$ (kN.m)	$M_{Bi,s}/M_{Bi,s}^{FE}$
1	1	2h	5.16	5.27	13.45	0.46	153.95	75.91	282.09	14.1	16.12	1.07
		4h	5.16	5.27	11.1	0.38	253.91	125.2	232.8	11.64	16.12	0.99
	2	2h	14.29	5.09	38.99	1.31	436.86	108.82	249.18	40.72	52.06	0.99
		4h	14.29	5.09	29.95	1.01	669.04	166.65	191.35	31.28	52.06	0.88
	3	2h	23.85	4.94	67.25	2.22	736.78	124.29	233.71	70	94.66	0.89
		4h	23.85	4.94	50.11	1.65	1090.2	183.91	174.09	52.16	94.66	0.87
2	1	2h	5.16	5.27	9.87	0.34	112.93	55.68	302.32	15.1	16.12	1.10
		4h	5.16	5.27	8.54	0.29	195.46	96.38	261.62	13.08	16.12	1.00
	2	2h	14.29	5.09	29.54	0.99	330.98	82.44	275.56	45.04	52.06	0.97
		4h	14.29	5.09	24.04	0.81	537.11	133.79	224.21	36.66	52.06	0.92
	3	2h	23.85	4.94	51.72	1.71	566.66	95.59	262.41	78.6	94.66	0.91
		4h	23.85	4.94	40.94	1.35	890.81	150.27	207.73	62.22	94.66	0.88
3	1	2h	5.16	5.27	7.39	0.25	84.58	41.7	316.3	15.8	16.12	1.09
		4h	5.16	5.27	6.62	0.23	151.46	74.68	283.32	14.16	16.12	1.02
	2	2h	14.29	5.09	22.62	0.76	253.4	63.12	294.88	48.18	52.06	0.95
		4h	14.29	5.09	19.25	0.65	429.94	107.09	250.91	41	52.06	0.93
	3	2h	23.85	4.94	40.06	1.32	438.89	74.04	283.96	85.06	94.66	0.90
		4h	23.85	4.94	33.28	1.1	724.05	122.14	235.86	70.66	94.66	0.89

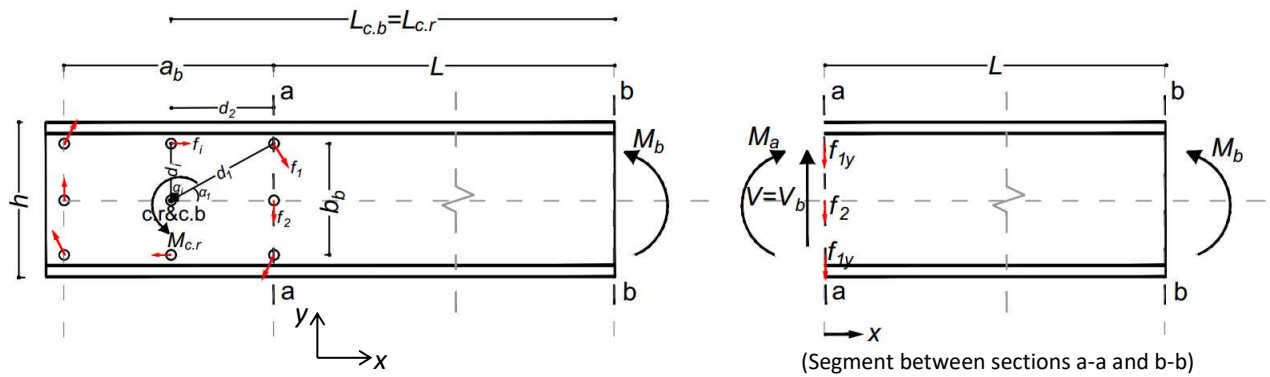
**Table 4.** Calculated cross-sectional dimensions, properties and flexural capacity of the optimised CFS bolted moment connections subject to bending at the beam end section

$a_b/h$	$t$ (mm)	$L$	$h$ (mm)	$b$ (mm)	$c$ (mm)	$\theta^\circ$	$I_{eff}$ $\times 10^6$ (mm <sup>4</sup> )	$\omega$ $\times 10^3$ (mm <sup>2</sup> )	$V$ (kN)	$T$ (kN.m)	$B$ (kN.m <sup>2</sup> )	$\sigma_B$ (MPa)	$\sigma_M$ (Mpa)	$M_{Bi}$ (kN.m)	$M_{M,EC3}$ (kN.m)	$M_{Bi}/ M_{Bi,s}$
1	1	2h	426	50	13	104	7.2	2.65	13.51	0.19	79.93	50.81	307.19	17.98	18.38	1.28
		4h	430	50	11	96	7.2	2.54	11.75	0.16	133.16	86.59	271.41	15.76	18.18	1.35
	2	2h	414	50	19	108	18.2	3.16	39.89	0.71	284.19	84.15	273.85	49.76	56.6	1.22
		4h	428	50	12	105	18.35	2.85	31.78	0.5	404.01	125.08	232.92	40.9	54.54	1.31
	3	2h	401	50	25	110	30.55	2.76	67.06	1.03	419.71	86.67	271.33	86.12	97.78	1.23
		4h	414	50	19	108	30.57	2.41	53.46	0.69	565.71	123.09	234.91	70.98	92.92	1.36
2	1	2h	427	50	13	93	7.2	2.61	9.67	0.13	56.52	36.69	321.31	18.2	18.36	1.21
		4h	428	50	12	104	7.21	2.6	8.76	0.12	101.65	64.96	293.04	17.1	18.3	1.31
	2	2h	406	50	23	99	18.05	3.24	30.15	0.56	219.03	66.91	291.09	53.94	57.74	1.20
		4h	422	50	15	103	18.33	2.97	24.82	0.41	328.64	100.99	257.01	46.02	55.68	1.26
	3	2h	393	50	29	108	30.29	2.93	50.74	0.83	333.99	68.3	289.7	93.54	99.6	1.19
		4h	408	50	22	107	30.66	2.54	41.73	0.57	464.79	99.72	258.28	79.92	95.22	1.28
3	1	2h	426	50	13	102	7.19	2.66	7.14	0.1	42.3	26.97	331.03	19.38	19.36	1.23
		4h	427	50	12	100	7.21	2.58	6.61	0.09	76.41	48.99	309.01	18.02	18.28	1.27
	2	2h	399	50	26	101	17.98	3.3	22.93	0.44	169.63	51.15	306.85	57.02	59.92	1.18
		4h	413	50	19	106	18.18	3.18	19.78	0.36	280.36	83.6	274.4	50.14	56.88	1.22
	3	2h	391	50	30	110	29.91	3.11	39.19	0.7	274.29	54.51	303.49	99.1	100.88	1.17
		4h	399	50	26	109	30.54	2.77	33.24	0.51	407.24	84.24	273.76	87	97.9	1.23

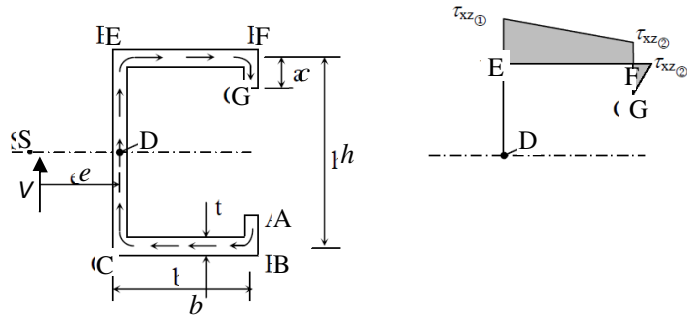
List of Figure



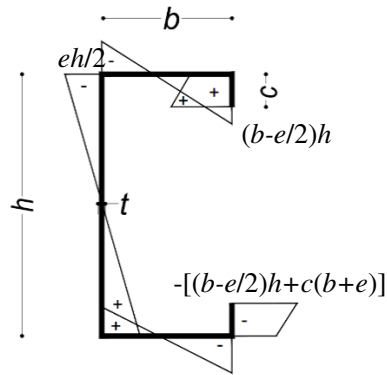
**Fig. 1.** Combined stress profile of a CFS lipped-channel section subjected to bending and bimoment (generated using CUFSM (Schafer, 2006))



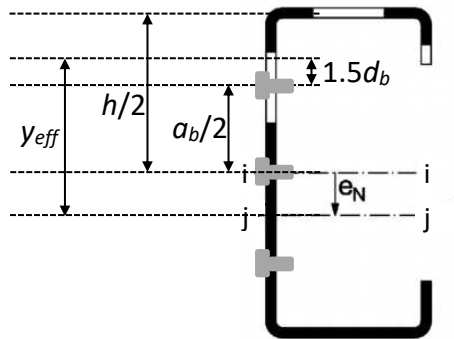
**Fig. 2.** Internal bolt-forces distributed uniformly caused by a pure bending moment



**Fig. 3.** Shear flow diagram in a CFS lipped-channel section caused by bolt-group forces

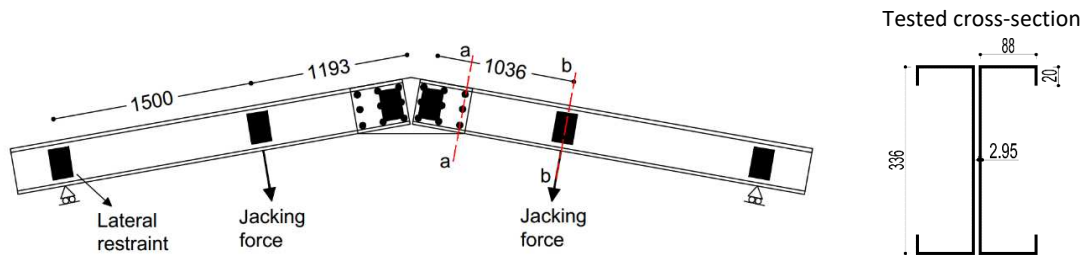


**Fig. 4.** The values of sectorial coordinate ( $\omega$ ) around the section

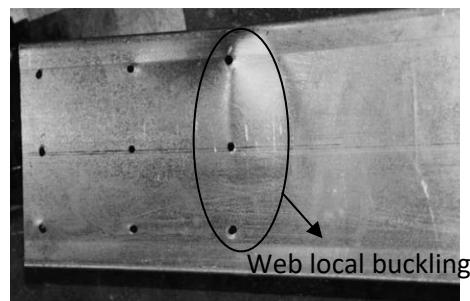


**Fig. 5.** Effective cross-section of a CFS beam

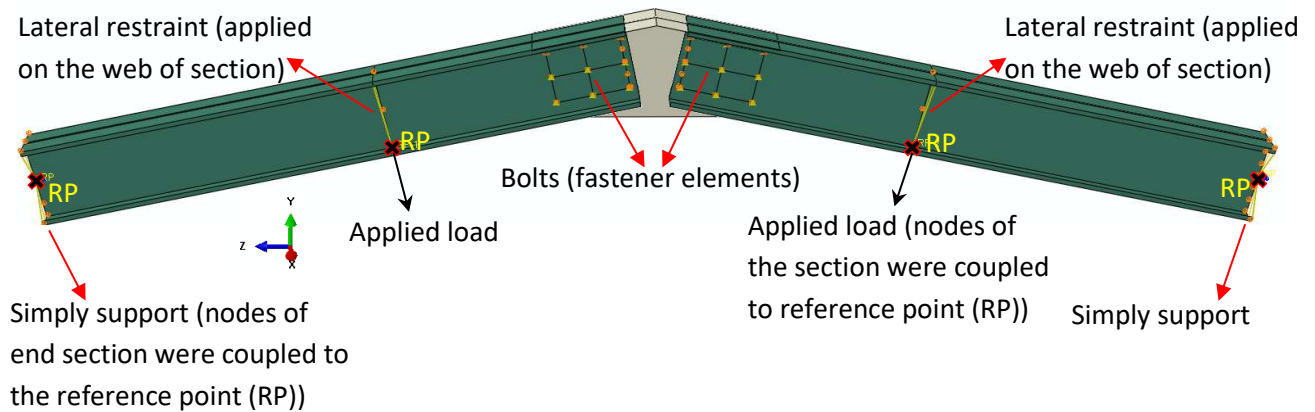




**Fig. 6.** Apex joint under four-point bending tested by Lim and Nethercot (2003) (dimensions in mm)



**Fig. 7.** Dominant failure mode of the apex joints tested by Lim and Nethercot (2003)



**Fig. 8.** FE model of the CFS bolted apex connection, including loading and boundary conditions

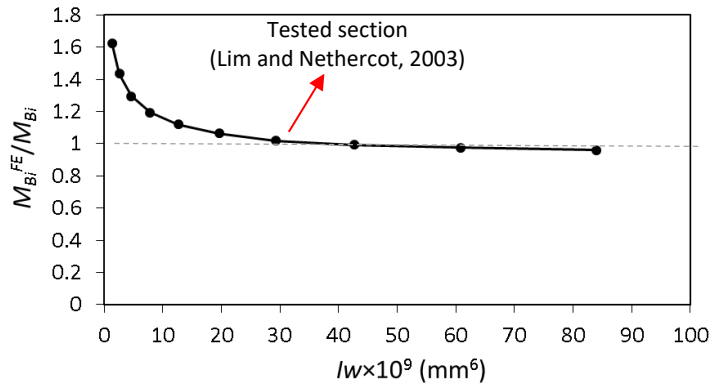


Fig. 9. Sensitivity study on the accuracy of the proposed analytical approach

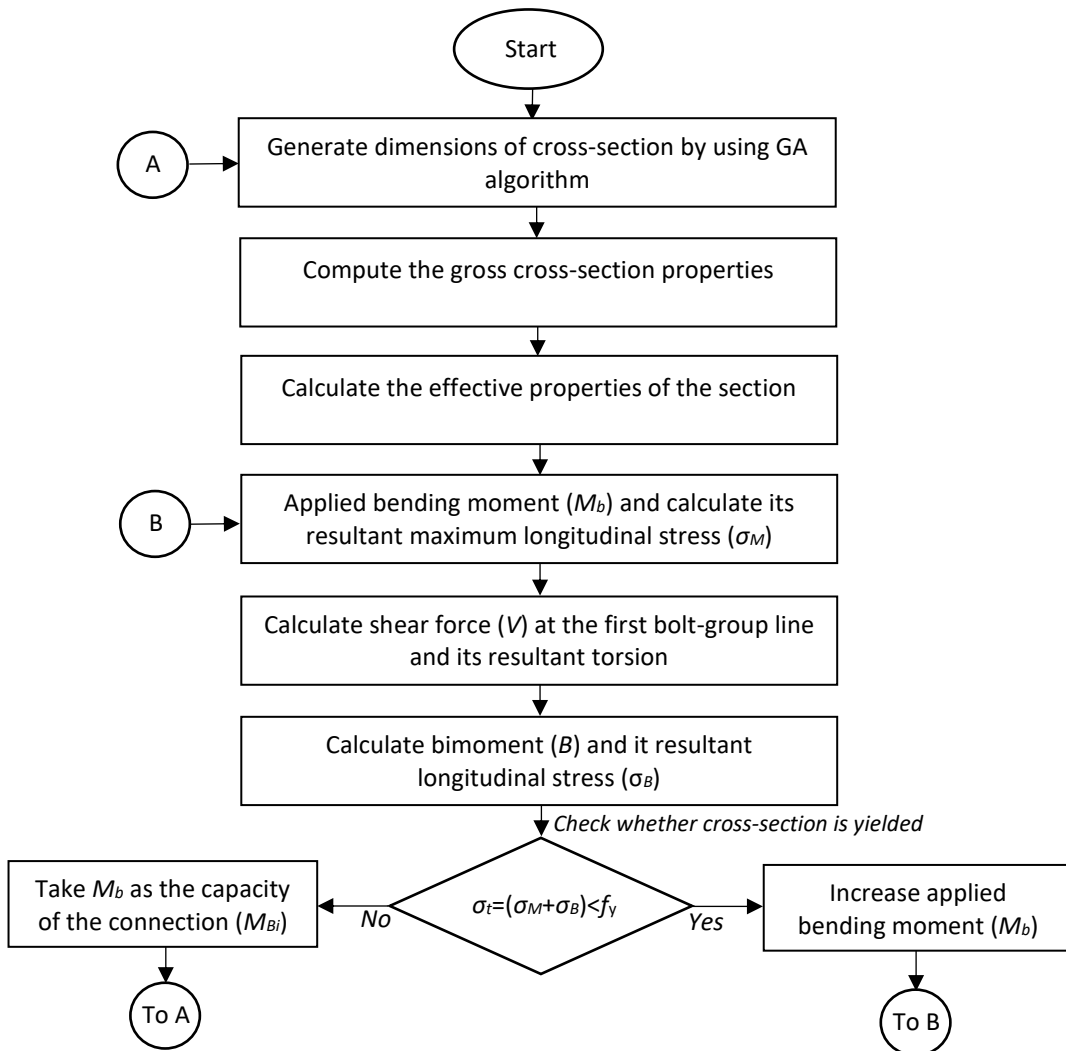


Fig. 10. Optimisation process flowchart of the beam section considering the effect of bimoment

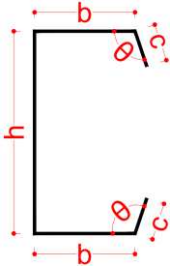
Lipped-channel	Design variables	Constraints based on EC3	Comments	Manufacturing & practical limitations (mm)
		$0.2 \leq c/b \leq 0.6$		
	$x_1 = c/b$	$b/t \leq 60$	EN1993-1-3 Table 5.1 and Equation (5.2a), Clause 5.5.3.2(1)	$400 \geq h \geq 100$
	$x_2 = b/L$	$c/t \leq 50$		$b \geq 50$
	$x_3 = \theta$	$h/t \leq 500$		$c \geq 10$
	$\pi/4 \leq \theta \leq 3/4\pi$			

Fig. 11. CFS beam with lipped sections, design variables and optimisation constraints


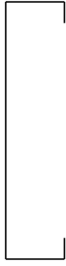




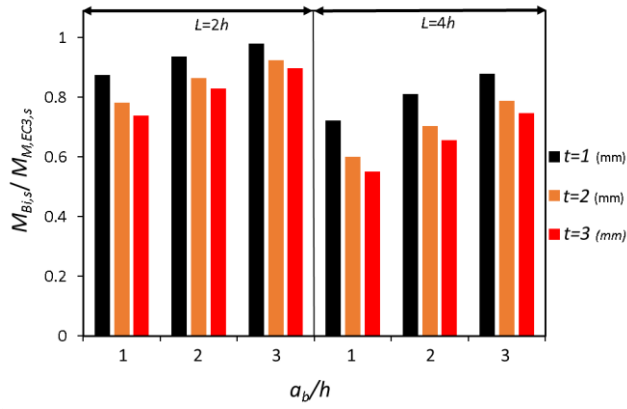
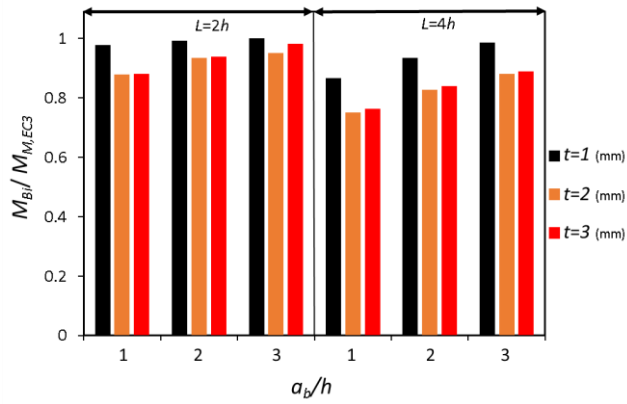
Tested cross-section	Optimised cross-section without bimoment	Optimised cross-section considering bimoment			
		Bolt-group length of test A	Bolt-group length of test B	Bolt-group length of test C	Bolt-group length of test D
		$a_b = 391 \text{ mm}$ ( $a_b/h = 0.94$ )	$a_b = 476 \text{ mm}$ ( $a_b/h = 1.16$ )	$a_b = 566 \text{ mm}$ ( $a_b/h = 1.38$ )	$a_b = 718 \text{ mm}$ ( $a_b/h = 1.83$ )
336×88×20 mm 	392×50×30 mm 	416×50×18 mm 	411×50×20 mm 	403×50×24 mm 	398×50×27 mm 
Improvement in flexural capacity of the optimised sections compared to the tested section	9%	24%	19%	16%	10%
$M_{Bi}$ (kN.m)	-	86.38	88.61	92.52	99.07
Accuracy of analytical approach compared to FE results ( $M_{Bi}/M_{Bi}^{FE}$ )	-	0.89	0.91	0.94	0.98

Fig. 12. Comparison between the tested (Lim and Nethercot, 2003) and optimised cross-sectional shapes



(a)



(b)

**Fig. 13.** The strength reduction of the (a) tested cross-section (300x88x20 mm) and (b) optimised cross-sections due to the effect of bimoment in CFS bolted moment connections